Published in final edited form as:

Nat Struct Mol Biol. 2022 August ; 29(8): 791–800. doi:10.1038/s41594-022-00808-5.

Yeast PI31 Inhibits the Proteasome by a Direct Multisite Mechanism

Shaun Rawson[1,2,*], **Richard M. Walsh Jr.**[1,2,*], **Benjamin Velez**[3], **Helena M. Schnell**[3], **Fenglong Jiao**[4], **Marie Blickling**[3], **Jessie Ang**[3], **Meera K. Bhanu**[3], **Lan Huang**[4], **John Hanna**[3,#]

[1]Harvard Cryo-Electron Microscopy Center for Structural Biology, Harvard Medical School, Boston, Massachusetts, United States of America

[2]Department of Biological Chemistry and Molecular Pharmacology, Blavatnik Institute, Harvard Medical School, Boston, Massachusetts, United States of America

[3]Department of Pathology, Harvard Medical School and Brigham and Women's Hospital, Boston, Massachusetts, United States of America

[4]Department of Physiology and Biophysics, University of California-Irvine, Irvine, CA, United States of America

Summary

Proteasome inhibitors are widely used as therapeutics and research tools, typically targeting one of the three active sites, each present twice in the complex. An endogeneous proteasome inhibitor, PI31, was identified 30 years ago but its inhibitory mechanism has remained unclear. Here we identify the mechanism of *S. cerevisiae* PI31, also known as Fub1. Using cryo-EM, we show that Fub1's conserved C-terminal domain is present inside the proteasome's barrel-shaped core particle where it simultaneously interacts with all 6 active sites. Targeted mutations of Fub1 disrupt proteasome inhibition at one active site, while leaving the other sites unaffected. Fub1 itself evades degradation through distinct mechanisms at each active site. The gate that allows substrates to access the CP is constitutively closed and Fub1 is enriched in mutant CP's with an abnormally open gate, suggesting that Fub1 may function to neutralize aberrant proteasomes, thereby ensuring the fidelity of proteasome-mediated protein degradation.

Keywords

proteasome; PI31; Fub1; core particle; bortezomib

[#]Corresponding Author: jwhanna@bwh.harvard.edu.
[*]These authors contributed equally.

Author contributions

J.H., B.V., H.M.S., M.B., J.A., and M.K.B. performed the biochemical aspects of the work. R.W. and S.R. performed cryo-EM sample preparation, data collection, data processing, model building and refinement while R.W., S.R., and H.M.S. performed the data analysis. F.J. and L.H. performed the cross-linking experiments. H.M.S, J.H., S.R., and R.W. prepared the figures. J.H. wrote the paper with assistance from H.M.S, R.W., and S.R., and input from all authors.

Competing Interests Statement

The authors declare that they have no conflict of interest.

Introduction

Regulated protein degradation is critical for cellular homeostasis. Protein quality control pathways identify and eliminate aberrant proteins, while targeted destruction of key regulatory proteins controls diverse cellular processes. The proteasome is a 2.5 MDa multisubunit complex that consists of a central core particle (CP) capped at either end by a regulatory particle (RP). The 700 kDa CP is composed of 4 stacked heptameric rings with an αββα configuration. Each β-ring houses 3 active sites (chymotryptic/β5, tryptic/β2, and post-acidic/β1) while each α-ring contains a gate that facilitates access of substrates to the CP interior. The RP binds, unfolds, and deubiquitinates substrates, but also opens the gate, allowing for insertion of the substrate into the CP [1].

There are ~35 integral subunits of the proteasome, most of which are required for its overall structure and are essential for viability. However, there are many additional proteasome-interacting proteins. Some of these proteins function as assembly chaperones, helping to orchestrate new proteasome biogenesis but being themselves excluded from the final proteasome product [2]. Others interact with mature proteasomes, sometimes sub-stoichiometrically and reversibly. These proteins regulate diverse aspects of proteasome function, including substrate processing, cellular localization, proteolytic activity, and others [3-10].

PI31 (also known as PSMF1 or Fub1) was identified in 1992 as an *in vitro* inhibitor of the CP [11]. It is highly conserved from yeast to humans, and human PI31 is capable of complementing the yeast *fub1Δ* mutant [12]. PI31 has activity against all three proteasome active sites[11,13]. Proteasome inhibition *in vitro* is mediated by PI31's C-terminal region, which is both necessary and sufficient for its inhibitory effect [12,14,15]. *In vivo*, loss of PI31's C-terminus recapitulates the null mutant phenotype while expression of the C-terminal region alone is sufficient to rescue the null mutant, confirming that this part of the protein is critical for PI31's cellular function [12,15]. Despite having been discovered 30 years ago, PI31's mechanism of proteasome inhibition remains unclear. One model, which would explain PI31's ability to inhibit all three CP active sites, is that PI31 sits atop the CP gate, blocking access of substrates.

Here we report a high-resolution cryo-EM structure of Fub1 in association with CP, revealing an unexpected mechanism of proteasome inhibition that operates through simultaneous and specific inactivation of all 6 active sites. Fub1 itself evades degradation by the proteasome through different mechanisms at each active site. Fub1 is enriched in mutant CP's with an open gate conformation, suggesting that Fub1 may have evolved to specifically recognize and neutralize aberrant CP species.

Results

Fub1 is Enriched in the *α3Δ* Mutant

We confirmed the key known features of Fub1, namely that it potently inhibits the CP *in vitro* (Fig. 1a) but is required for resistance to proteotoxic stress *in vivo* (Fig. 1b). We examined whole cell extracts under the same proteotoxic stress conditions as in Fig. 1b, and

found increased proteasome activity in the *fub1Δ* mutant relative to wild-type (Extended Data Fig. 1a). There was no difference in proteasome levels under these conditions (Extended Data Fig. 1b), suggesting that Fub1 also inhibits the CP *in vivo*.

We next examined the distribution of Fub1 in whole cell extracts from wild-type cells under steady-state conditions (i.e. non-stress) by size exclusion chromatography. Almost all Fub1 migrated at a size consistent with a homodimer (~60 kDa) with little Fub1 co-eluting with CP or proteasome holoenzyme (Fig. 1c). In the course of analyzing an *α3Δ* mutant, we noticed that the fraction of Fub1 co-eluting with proteasome was substantially increased (Fig. 1c). α3 (also known as Pre9) is the only non-essential CP subunit, and its loss is tolerated only because a second copy of α4 is able to take the place of the missing subunit [16]. Because α3 is a major contributor to the CP gate, its absence results in a constitutively open gate [16,17]. Previous work showed that Fub1 preferentially binds free CP with little or no binding to RP-CP species [15]. Our data are consistent with this finding as the peak of proteasome-bound Fub1 appeared to coincide with the peak of free CP, which runs around fractions 13-15 on this column (Fig. 1c). Interestingly, RP-CP species were actually somewhat enriched in the *α3Δ* mutant relative to wild-type (Fig. 1c), although we did not study this finding further.

We affinity purified CP from the *α3Δ* mutant using a genomically integrated C-terminal TEV-ProA tag on Pre1 (β4). Fub1 was highly enriched in purified *α3Δ* CP (Fig. 1d). The strength of the Fub1-CP interaction is underscored by the stringent wash conditions (500 mM NaCl) required to separate RP from CP. Fub1 was present in free CP as well as two higher molecular weight species. Both of the heavier species were eliminated by deletion of Blm10 (Extended Data Fig. 2), a poorly understood CP regulator that binds to the surface of the α-ring in a manner similar to RP [18,19]. Interestingly, we did not detect doubly Blm10-capped CP by cryo-EM analysis (Extended Data Fig. 3).

Fub1 is Present Within the CP Barrel in *α3Δ* Mutants

We determined the structure of *α3Δ* CP by cryo-EM to a resolution of 2.7 Å (Fig. 2a,b; Extended Data Fig. 3; Table 1). Molecular modeling confirmed a second copy of α4 at the position normally occupied by α3, as well as a constitutively open CP gate (Fig. 2c,d). There was no evidence of an assembly defect in the CP: specifically, there was no density corresponding to any of the five CP chaperones or the five β-subunit propeptides, which are cleaved before final maturation of the proteasome.

Quite unexpectedly, a subset (~18%) of the particles showed a substantial novel density within the CP interior (Fig. 3a and Extended Data Fig. 3,4). We determined the structure of this subset of CP particles to a resolution of 3.0 Å. Molecular modeling revealed the density to be the C-terminal half of Fub1 (residues 127-229; Fig. 3a) which was present as a dimer at the β/β-ring interface and which showed an extended conformation largely lacking secondary structure. The modeled density began near β1 and then traversed the center of the ring towards β5 where it dimerized with the second copy of Fub1 (Fig. 3b-d). The first copy of Fub1 then returned across and over into the opposing β-ring where it contacted the second Fub1 in the vicinity of the other β5 subunit. Finally, Fub1 descended back into the first β-ring where the modeled density terminated in front of β2 (Fig. 3b-d). An

early observation about PI31 was the proline-rich nature of its C-terminus [14]. Our structure explains this finding as many of these prolines facilitate the sharp turns needed to wind around the β-rings.

The most striking feature of this structural arrangement was that it brought Fub1 density into close contact with all 6 proteasome active sites (Fig. 3b and Fig. 4). These regions are by far the most evolutionarily conserved (Supplementary Information Fig. 1), suggesting that they are critical for Fub1 function. Their position, occupying and filling each of the active site pockets, would be expected to inhibit the proteasome. Indeed, Fub1's position within the β5 pocket mirrored that of the proteasome inhibitor bortezomib (Fig. 4a,b), which is a modified Phe-Leu dipeptide with a C-terminal boronic acid electrophile. Bortezomib's hydrophobic Phe-Leu portion directs the compound to the β5 active site pocket, while the boronate group covalently binds to the active site Thr76, with additional hydrogen bonds to Thr76 and Gly122 (Fig. 4a). As noted above, both Fub1 molecules come together to occupy the β5 pocket. A group of hydrophobic residues (Met198, Ile199, and Phe200) fills the pocket (Fig. 4b). Meanwhile, Asp170 from the other Fub1 molecule forms hydrogen bonds with β5 Thr76 and β5 Gly122 (both similar to bortezomib) as well as β5 Ser206 (Fig. 4b).

At the β1 active site, a group of acidic residues fills the pocket with Fub1 Asp130 hydrogen bonded to the active site Thr20, as well as β1 Ser187 and β1 Thr40 which further enforce this positioning (Fig. 4c). Fub1 Glu132 is also hydrogen bonded elsewhere in the pocket (Fig 4c). Fub1 does not directly interact with the β2 active site threonine, but is engaged in multiple hydrogen bonds throughout the active site pocket which appear to help stabilize this segment of Fub1 there (Fig. 4d). Thus Fub1 directly binds and fills each of the active site pockets.

Fub1 Specifically Inhibits All Three Proteasome Active Sites

The three CP active sites can be individually monitored using fluorogenic substrates. Our structure predicts that targeted mutations of Fub1 should disrupt proteasome inhibition at one active site, while leaving the other two active sites unaffected. The hydrophobic residues Phe129 and Tyr133 help to enforce the overall position of this segment of Fub1 at the β1 active site (Fig. 4c). A Fub1-F129A/Y133A mutant showed near total abrogation of inhibition at the β1 active site, which cleaves after acidic residues, but had no effect on the β2 and β5 active sites, which mediate the tryptic and chymotryptic activities, respectively (Fig. 5a-c). Similarly, Fub1-M198A/F200A showed substantial loss of inhibition of the β5 active site (Fig. 5e) but had no effect on β2 (Fig. 5f) and only a modest loss of inhibition at β1 (Fig. 5d). Note that CP treated with Fub1-M198A/F200A showed ~3-fold loss of inhibition of the β1 active site (Fig. 5d), but nearly 50-fold loss of inhibition at the β5 active site (Fig. 5e). In the vicinity of the β2 active site, the Fub1 segment was folded back on itself, suggesting that a small peptide might have enough structure to bind and fill the active site pocket. We synthesized a 20-residue peptide (residues 213-232) which was sufficient to completely inhibit β2 activity, but again had no effect on the other two active sites (Fig. 5g-i). The IC50 was <10 μM. Proline-containing sequences at either end of this peptide were necessary for maximal inhibition (Extended Data Fig. 5). Note that these peptide hydrolysis

assays require a small amount of detergent which opens the CP gate allowing substrate to enter. Naturally, this also provides a potential portal of entry for Fub1.

Next, we sought to determine the physiologic significance of these interactions by expressing a Fub1 mutant compromised for inhibition at 2 of the 3 active sites (β5 and β1) in the *fub1Δ* background. This mutant was unable to complement the *fub1Δ* mutant *in vivo* (Fig. 5j), confirming the importance of these inhibitory interactions. This effect was not due to decreased protein levels of mutant Fub1. These results strongly substantiate the assignment of Fub1 to the novel central density in *α3Δ* (see also Fig. 3c,d), explain its proteasome-inhibitory mechanism *in vitro*, and establish a paradigm for complete proteasome inhibition with specificity at all 6 sites.

Fub1 Evades Degradation by the Proteasome

Given its proximity to the proteasome's active sites, we next asked whether Fub1 itself was subject to degradation. In principle, our ability to obtain a Fub1-CP structure suggests that this should not be the case since resolution in the cryo-EM method requires Fub1 to be largely fixed in its position. We examined this issue directly using the cycloheximide chase assay. Fub1 was completely stable over a 90 minute time course (Fig. 6a), comparable to the CP subunit α5 and in contrast to a known short-lived protein, Tmc1[20]. Note that the steady-state level of Tmc1 is increased in the *α3Δ* mutant, consistent with prior work [21].

We then modeled Fub1 onto existing structures of CP bound to peptide proteasome inhibitors [22,23] to establish which Fub1 residues were in the P3-P2-P1-P1'-P2'-P3' positions (where the scissile bond is between P1 and P1'). At the β5 active site, Met198 was in the P1 position while Asp170 occupied P1' (Fig. 6b). However, because these residues derive from different chains of the Fub1 dimer, there is no peptide bond to cleave, helping explain how Fub1 evades degradation at this site. In effect, Fub1 resembles an already cleaved substrate that cannot be released due to its extensive interactions throughout the active site (Fig. 4b). Two features likely contribute to Fub1's stability in the β2 site. First, the P1 position is occupied by Asp224, which is unfavorable for β2 since it prefers to cleave after basic residues (Fig. 6c). Second, the Fub1 polypeptide main chain is quite far from the active site threonine (~5.7 Å), and this is likely incompatible with nucleophilic attack. This latter effect essentially creates a cap-like structure over the active site. At the post-acidic β1 active site, Fub1 does present acidic residues (Fig. 6d). However, the Fub1 polypeptide is actually oriented in the reverse direction (COOH-to-NH_2) relative to other β1 peptide inhibitors. This backwards orientation appears likely to prevent proteolysis, which requires precise positioning of the active site on the substrate. Furthermore, as with β2, the potential scissile bond is far from the active site threonine (~6.9 Å). Thus, Fub1 appears to take three distinct approaches to thwart its own degradation.

Fub1 Recognizes Proteasomes with an Aberrant CP Gate

The *α3Δ* mutant shows both a constitutively open gate and aberrant CP composition. In principle, an abnormally open gate could facilitate insertion of Fub1's unstructured C-terminus. To separate the effects of an open gate and abnormal composition, we examined a mutant with small deletions of the N-termini of α3 and α7 (residues 2-10 and 2-12,

respectively) [24]. This mutant has an open gate (Fig. 7a) but otherwise normal α-ring composition. Similar to *α3Δ*, the *α3ΔN α7ΔN* CP showed marked enrichment for Fub1 (Fig. 7b), suggesting that a constitutively open gate may be a key feature contributing to Fub1's association with CP.

Fub1's N-terminal Domain Appears to Sit Atop the CP

Unlike its C-terminus, the N-terminus of PI31 forms a well-folded globular domain [25]. We were unable to resolve Fub1's N-terminus in our reconstruction. We therefore turned to cross-linking mass spectrometry [26]. We identified six Fub1-CP crosslinks, all of them involving the α-ring and the N-terminal half of Fub1 (Fig. 7c; Supplementary Data Table 1). Five of these cross-links involved residues on the outer surface of the α-ring (α4-K28, α4-K53, α4-K169, α5-K66, and α2-K166). The last residue, α4-K88, is actually inside the CP barrel, but its distance from the α-ring surface is still well within the cross-linkable distance. No cross-links were detected within Fub1's C-terminus. Furthermore, through the application of a low pass filter, we were able to identify additional density on the outer surface of the CP in our Fub1-bound cryo-EM reconstruction (Fig. 7d). Although the low resolution precluded molecular modeling, this density was not present in the *α3Δ* CP lacking Fub1. Additional low resolution density could be identified transiting through the CP barrel through the α-ring and into the β-ring (Extended Data Fig. 6). Together, these data suggest that Fub1's N-terminus remains outside and atop the CP on the surface of the α-ring, while its unstructured C-terminus enters the CP interior.

Evolutionary Conservation of Proteasome Inhibition by PI31/Fub1

Finally, we examined the evolutionary conservation of PI31/Fub1's ability to inhibit the CP *in vitro*. Human PI31, expressed and purified from bacteria, inhibited yeast CP (Fig. 7e). Conversely, yeast Fub1 inhibited human CP (Fig. 7f). Interestingly, yeast Fub1 inhibited yeast CP more effectively than human PI31, and human PI31 inhibited human CP better than yeast Fub1, suggesting that Fub1 and PI31 are each specifically adapted to their own species's CP. Thus, the function of PI31/Fub1 is highly conserved both *in vitro* (Fig. 7e,f) and *in vivo* [12,15].

Discussion

PI31's Mechanism of Proteasome Inhibition

Inhibition of the proteasome was the first known aspect of PI31 function and the property that led to its identification in 1992[11]. However, its mechanism of proteasome inhibition remained unknown until now. The ability of PI31 to compete with RP for binding to CP *in vitro*[13] suggested that PI31 might bind the outer surface of the α-ring. Thus, the leading model of CP inhibition had Fub1 bound to the surface of the α-ring, blocking access of substrates to the proteasome gate through either a capping or plugging mechanism, thereby explaining PI31's surprising ability to inhibit all 3 types of active site.

In contrast to this model, we show that Fub1 simultaneously inhibits each of the proteasome's 6 active sites through direct and extensive interactions with the active site pockets, an arrangement that requires Fub1 to access the CP interior. Thus, Fub1 is

conceptually similar to modified peptide inhibitors of the proteasome such as bortezomib that work by direct interaction with the active sites[22]. However, unlike bortezomib and related FDA-approved drugs that target only the chymotryptic site at physiologically relevant concentrations, Fub1 has found a way to inhibit all 6 active sites simultaneously. Also unlike bortezomib, Fub1 achieves potent proteasome inhibition without the aid of an electrophilic warhead. It will be important to determine if human PI31 operates through a similar mechanism. Human PI31 can rescue the yeast *fub1Δ* mutant *in vivo* [12,15] and inhibits yeast CP *in vitro* (Fig. 7e,f), suggesting that the detailed mechanisms of PI31 and Fub1 may be closely related.

Like most protein inhibitors of proteases, Fub1 works by preventing access of substrates to the active sites [27]. Fub1's ability to do this requires it to bind the active sites in a substrate-like manner (Fig. 4) but then evade degradation (Fig. 6), which Fub1 appears to do through different mechanisms at each active site. Some of these mechanisms, including splitting the P1/P1' residues into different polypeptides, appear unprecedented to our knowledge.

The very presence of Fub1 inside the CP raises the question of how it got there. One possibility is that Fub1 accesses the β-rings when they are exposed during CP assembly, obviating the need to traverse the gate. This seems unlikely for two reasons. First, our purified *α3Δ* CP appears mature with no evidence of an assembly defect. Second, the position of Fub1 appears incompatible with immature CP as it would clash with β-subunit propeptides [28]. Thus, it seems most likely that Fub1 associates with mature CP and therefore must enter the CP chamber through its only point of entry, its central gate. We suspect that Fub1's initial recognition of the CP occurs on the outer surface of the α-ring, and the unstructured nature of Fub1's C-terminal domain then facilitates entry into the CP interior. There are some unresolved regions within the Fub1 structure (Fig. 3a). While such gaps often reflect flexible regions, a second possibility is that they reflect partial proteolysis of Fub1 within the CP chamber. However, the stability of Fub1 *in vivo* makes this less likely (Fig. 6a).

In contrast to the C-terminal domain, the N-terminal domain is highly structured [25,29] but shows little or no binding to CP on its own [30]. Thus, its position may be flexible, potentially explaining why it was not well resolved in our reconstruction. Nevertheless our cross-linking data and low-resolution structural analysis suggest that it remains on the surface of the α-ring. This is consistent with the fact that it is too large in its folded state to transit through even the *α3Δ* pore. This arrangement would also help explain the preference of Fub1/PI31 for CP over RP-CP and its ability to compete with RP for CP binding *in vitro* [14]. We do not yet understand the structure of Fub1 as it transits through the CP gate as these areas of Fub1 were not resolved. Nevertheless, it is worth noting that the CP's ability to carry out endoproteolytic cleavage of substrates suggests that at least two polypeptide chains may transit through the CP pore[31].

Physiologic Function of Fub1/PI31

PI31/Fub1's ability to inhibit the CP *in vitro* is well documented. Our data suggest that Fub1 also inhibits the proteasome *in vivo* as our Fub1-CP structure reflects endogenous untagged Fub1 bound to proteasome purified directly from cells. What then could account

for an inhibitory function of Fub1 in what appears to be an overall protective role against proteotoxic stress? A defining feature of proteasome-mediated degradation is its exquisite specificity. Given the proteasome's constitutively closed gate [32], substrates can only access the CP interior through the mediation of an activating complex like the RP. CP's with a constitutively open gate therefore represent a threat to the selectivity and fidelity of proteasome activity. Since the proteasome regulates myriad aspects of cell biology, such unregulated protein degradation would be expected to cause significant cellular dysfunction. One possibility is that Fub1 has evolved to recognize and neutralize dysfunctional proteasomes, particularly those with an aberrant or constitutively open gate, such as may arise from errors in CP subunit incorporation. Indeed, the larger the size of the pore defect, the easier it might be for Fub1's unstructured C-terminus to gain access to the CP interior, in effect enriching Fub1 in CP in proportion to the degree of aberrancy. According to proteome-wide protein abundance measurements, the typical CP subunit is present in cells at much higher levels than Fub1 [33]. The low abundance of Fub1 would be consistent with this sort of regulatory function. It is not known how often such aberrant CP's arise during normal CP biogenesis. Even if rare, the cellular threat could be substantial, potentially explaining the need for this kind of neutralizing activity. Understanding the cellular conditions and stimuli that induce proteasome binding by Fub1 represents an important goal for future work.

Previous models have suggested that PI31 promotes CP-RP association to facilitate the final step of proteasome biogenesis [34]. However, other groups have failed to detect a defect in proteasome assembly upon PI31 knockdown or in Fub1 mutants [15,30]. Our data make such a function for Fub1 unlikely because inhibition by Fub1's C-terminal region would render those CP ineffective for protein degradation. We do not see evidence of significant Fub1 turnover, and it is hard to see how Fub1 could easily be released given its extensive interactions within the CP. A second model proposes that PI31 serves as a proteasome transport factor [35]. Our data pose similar challenges for this model, although it should be noted that these models were developed in species other than yeast, and there could be species-specific differences in PI31 function.

In conclusion, our data explain how Fub1/PI31 inhibits the proteasome, addressing one of the oldest unanswered questions in the proteasome field and establishing a highly unexpected mechanism of proteasome inhibition. These data also establish Fub1 as one of the most sophisticated protein inhibitors of a protease ever described. There is still much to learn about Fub1/PI31's specific cellular roles, its regulation, and its association with neurodegenerative disease [36,37]. The data presented here should inform future work on these and other aspects of PI31 biology.

Methods

Strains, Plasmids, and Antibodies

Yeast strains and plasmids are listed in Supplementary Data Tables 2 and 3. Yeast strains were generated by standard homologous recombination-based methods. Yeast were cultured at 30°C or 37°C in YPD or synthetic media, as indicated. YPD medium consisted of 1% yeast extract, 2% Bacto-peptone, and 2% dextrose. Synthetic media consisted of 0.7% Difco

Yeast Nitrogen Base supplemented with amino acids, adenine, and 2% dextrose. Uracil was omitted from this medium for plasmid selection. Yeast strains were verified by PCR and/or immunoblotting.

Full-length Fub1 was cloned into pET45b which provides for an N-terminal 6x-histidine tag (pMB30), expressed in *E. coli*, and affinity purified to near homogeneity by Nickel chromatography. The purified protein was used to generate a rabbit polyclonal antibody. Anti-Pba1/2 [38] and anti-Alpha5 antibodies [28] have been previously described. Anti-Blm10 antibody was obtained from Enzo Life Sciences (BML-PW0570-0025) and anti-Pgk1 from Fisher Scientific (459250). The following dilutions were used: Fub1 (1:4000), Alpha5 (1:5000), Pba1/2 (1:4000), Blm10 (1:2000), and Pgk1 (1:2500).

Fub1 was also cloned into ycPlac33, a URA3-marked low-copy centromeric plasmid which expresses untagged Fub1 from its endogenous promoter sequences (500 bp upstream and 200 bp downstream; pJH155).

Point mutations in Fub1 plasmids were generated using the QuikChange Multisite-Directed Mutagenesis method (Agilent). Plasmids were verified by DNA sequencing.

Human PI31 was cloned into pGEX-4T-1 which provides for an N-terminal thrombin-cleavable GST-tag. The protein was expressed in *E. coli*, affinity purified by glutathione-sepharose chromatography, and eluted by thrombin cleavage.

Analysis of Whole Cell Extracts

Extracts were prepared from late-logarithmic phase cultures. Cells were resuspended in 50 mM Tris pH 8.0, 1 mM, EDTA, 5 mM $MgCl_2$, 1 mM ATP; lysed by French press; and centrifuged at 16,000xg for 25 min. Clarified lysates were then analyzed by size exclusion chromatography using a Superose 6 column.

CP Purification and Analysis

Proteasome was affinity purified via a genomically integrated C-terminal Pre1-TEV-ProA tag using IgG resin (MP Biomedicals; ICN55961), and CP was isolated using high salt (500 mM NaCl) washes as previously described [39]. Purified proteasomes were analyzed by standard SDS-polyacrylamide gel electrophoresis (PAGE) followed by Coomassie staining or immunoblotting. Naive gel analysis was performed using 3-8% Tris-Acetate gels (Invitrogen), followed by Coomassie staining or immunoblotting. Purified human 20S proteasomes were obtained from Enzo Life Sciences (BML-PW8720).

In Vitro Proteasome Activity Assays

Purified proteasomes (15 nM) were pre-incubated on ice for 20 min in the presence or absence of purified Fub1 present at 25-fold molar excess (considering Fub1 as a homodimer). CP-Fub1 mixtures were then incubated with the appropriate fluorogenic peptide at 30°C. SDS (0.02%) was provided in all assays to open the constitutively closed gate except for the indicated samples in Fig. 7A. Reactions were quenched by the addition of 1% SDS, and fluorescence was measured using a fluorometer. Suc-LLVY-AMC (Bachem I-1395) measures the proteasome's chymotryptic activity (β5) and was used at 100 μM with

a 20 minute reaction time. Boc-LRR-AMC (Bachem I-1585) and z-LLE-AMC (Bachem I-1945), which measure the tryptic (β2) and post-acidic (β1) activities respectively, were used at 300 μM with a 45 minute reaction time. Note that ~50% CP inhibition can be achieved with just 2-fold molar excess of Fub1. Fub1 peptides were synthesized by EZBiolab (Parsipanny, NJ) and reconstituted in water. In all assays, controls lacking CP were used to establish background/non-specific fluorescence.

Phenotypic Analysis of Yeast Mutants

Yeast cultures were grown overnight at 30°C in selective media, normalized by optical density, spotted in three-fold serial dilutions onto the indicated media, and incubated at 37°C for the indicated times.

Cryo-EM Sample Preparation

Sample preparation was performed as previously described[28], with additional and specific details provided here. CP that had been affinity purified was concentrated and injected over a Superose 6 10/300 GL column (GE Healthcare) that had previously equilibrated in SEC buffer (50 mM Tris, pH 7.5, 1 mM EDTA, and 100 mM NaCl). The CP-containing fractions were pooled and concentrated to ~1.8 mg/mL. Immediately prior to disposition onto 400 mesh Quantifoil Cu 1.2/1.3 grids that had been glow discharged in a PELCO easiGLOW (Ted Pella) at 0.39 mBar, 15 mA for 30 s, 3 μL of sample was mixed with 0.5 μL of a 3.5 mM Fos-Choline, fluorinated solution (Anatrace). Fos-Choline, fluorinated solution was used at a final concertation of 0.5 mM to diversify the particle orientations in ice. Samples were then vitrified in 100% liquid ethane using a Vitrobot Mark IV (Thermo Fisher Scientific), with a wait time of 15 s, blot time of 8 s, and a blot force of 20 at 100% humidity.

Cryo-EM Data Collection and Processing

Data collection and processing were performed as previously described[28], with additional and specific details provided here. Cryo-EM data were collected on a 300 kV Titan Krios G3i Microscope (Thermo Fisher Scientific) which was equipped with a K3 direct electron detector (Gatan) and a GIF quantum energy filter (25 eV) (Gatan) using counted mode at the Harvard Cryo-Electron Microscopy Center for Structural Biology at Harvard Medical School. Data were acquired utilizing image shift and real-time comma correction by beamtilt using the automated data collection software SerialEM [40]; nine holes were visited per stage position and a single movie was acquired per hole. Details of the data collection and dataset parameters are summarized in Table 1. Dose-fractionated images were gain normalized, aligned, dose-weighted, and summed using MotionCor2 [41] Contrast transfer function (CTF) and defocus value estimation were performed using CTFFIND4 [42]. Details of the data processing strategy are shown in Extended Data Fig. 3 and 4. Briefly, particle picking was carried out using crYOLO [43] followed by initial 2D classification within Relion [44] to give 953,049 particles. Heterogeneous classification in cryosparc [45] was used to sort particles into 20S or Blm10-containing groups or into “junk” classes which identified 310,494 20S particles. The 20S particles underwent Bayesian particle polishing and CTF refinement within Relion 3.1, and then further 3D classification using symmetry relaxation which identified 56,069 20S particles containing an unknown central density

(which ultimately proved to be Fub1). This resulted in a 3.0 Å reconstruction following subsequent rounds of CTF refinement and non-uniform refinement within cryosparc with C2 symmetry imposed (3.2 Å C1). Additionally, empty 20S classes were identified, the best of which underwent CTF refinement and non-uniform refinement in cryosparc resulting in a 2.7 Å C2 reconstruction from 150,227 particles (2.9 Å C1). Structural biology applications used in this project were compiled and configured by SBGrid [46].

Model Building and Refinement

The higher resolution 20S *α3Δ* model was built first using 7LS5 as a starting model. The duplicate α4 subunits were superimposed onto α3 of the starting model and then rigid body fit into the density. For both models, components were first rigid body fit into the electron density using UCSF Chimera (or Chimera X) [47]. This was followed by iterative cycles of manual building and refinement using Coot [48] and ISOLDE [49] for manual building, and Phenix [50] for real space refinement. The portion of the Fub1 density located near the CP ß2 subunit was built *de novo*; anchor regions for remaining portions were identified using DeepTracer [51] and manually rebuilt in Coot. 20S *α3Δ* and 20S *α3Δ* + Fub1 complexes were subjected to the same iterative process of manual building and refinement.

Sequence Analysis of Evolutionary Conservation

Evolutionary sequence conservation was analyzed using Consurf [52,53]. Comparison of full-length yeast and human sequences was done with Clustal Omega.

Cross-linking Mass Spectrometry

Affinity-purified *α3Δ* CP (~1.9 μM) was cross-linked with DSSO at a molar ratio of 1:100 (protein to linker) for 1h at room temperature [26]. After quenching with 50 mM NH_4HCO_3 for 10 min, cross-linked CP complexes were transferred onto a 30 KDa FASP centrifugal filter for protein digestion as described [54]. Cross-linked proteins were digested by Lys-C/Trypsin, Trypsin/Chymotrypsin, Lys-C/Chymotrypsin and Lys-C/Glu-C, respectively. For Lys-C/Trypsin digestion, samples were first digested by Lys-C (enzyme to protein ratio at 1:100) at 37°C for 4 h in 8M urea/25mM NH_4HCO_3 buffer, followed by trypsin digestion (enzyme to protein ratio of 1:50) in 1.5 M urea at 37°C overnight. For Trypsin/Chymotrypsin digestion, samples were dissolved in 25mM NH_4HCO_3 buffer containing 10mM $CaCl_2$ and digested by trypsin (enzyme to protein ratio of 1:100) and Chymotrypsin (enzyme to protein ratio of 1:100) at 37°C overnight. For Lys-C/Chymotrypsin digestion, samples were first digested by Lys-C (enzyme to protein ratio at 1:100) at 37°C for 4 h in 8M urea/25mM NH_4HCO_3 buffer, followed by Chymotrypsin digestion (enzyme to protein ratio at 1:50) in 25mM NH_4HCO_3 buffer containing 1.5 M urea and 10 mM of $CaCl_2$ at room temperature overnight. For Lys-C/Glu-C digestion, samples were first digested Lys-C (enzyme to protein ratio at 1:100) at 37°C for 4 h in 8M urea/25mM NH_4HCO_3 buffer, followed by Glu-C (enzyme to protein ratio at 1:100) in 25 mM NH_4HCO_3/1.5 M urea at 37°C overnight. The resulting peptides were extracted, desalted and separated by peptide SEC, and analyzed by LC MS^n as described [54]. MS^3 data were searched in Batch-Tag of Protein Prospector (v. 6.4.23). DSSO cross-linked peptides were identified at ≤ 0.19% FDR through the integration of MS^n data using an in-house script XL-Tool [54].

Extended Data

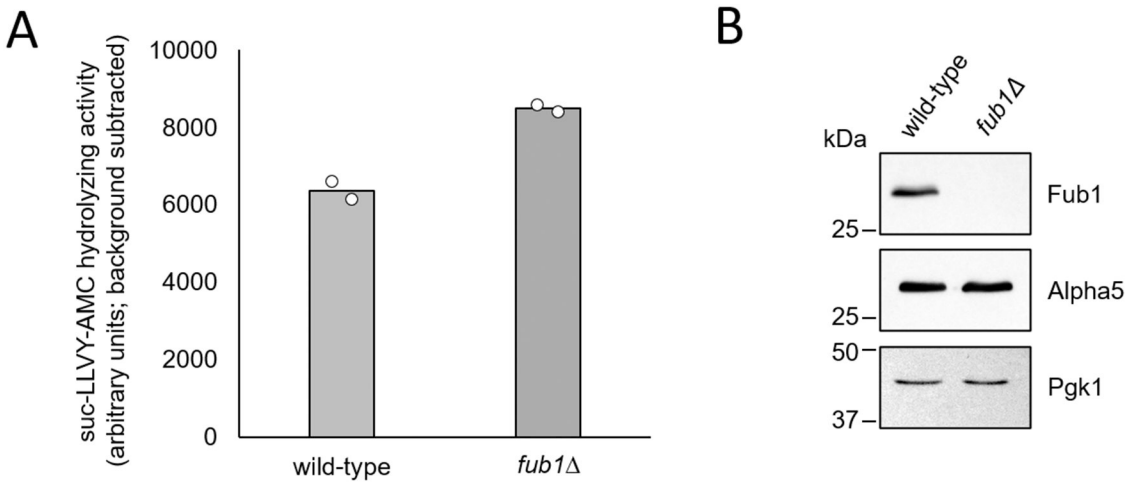

Extended Data Fig. 1. Proteasome Activity in Whole Cell Extracts.

a, Proteasome activity in whole cell extracts from wild-type and *fub1Δ* cells, as determined using the fluorogenic substrate suc-LLVY-AMC. Open circles indicate individual data points from biologic replicates. **b**, Proteasome levels are comparable in whole cell extracts. Extracts were prepared and analyzed by SDS-PAGE followed by immunoblotting with indicated antibodies. Alpha5 is a CP subunit while Pgk1 represents a loading control. Uncropped images for panel b and data for panel a are available as source data.

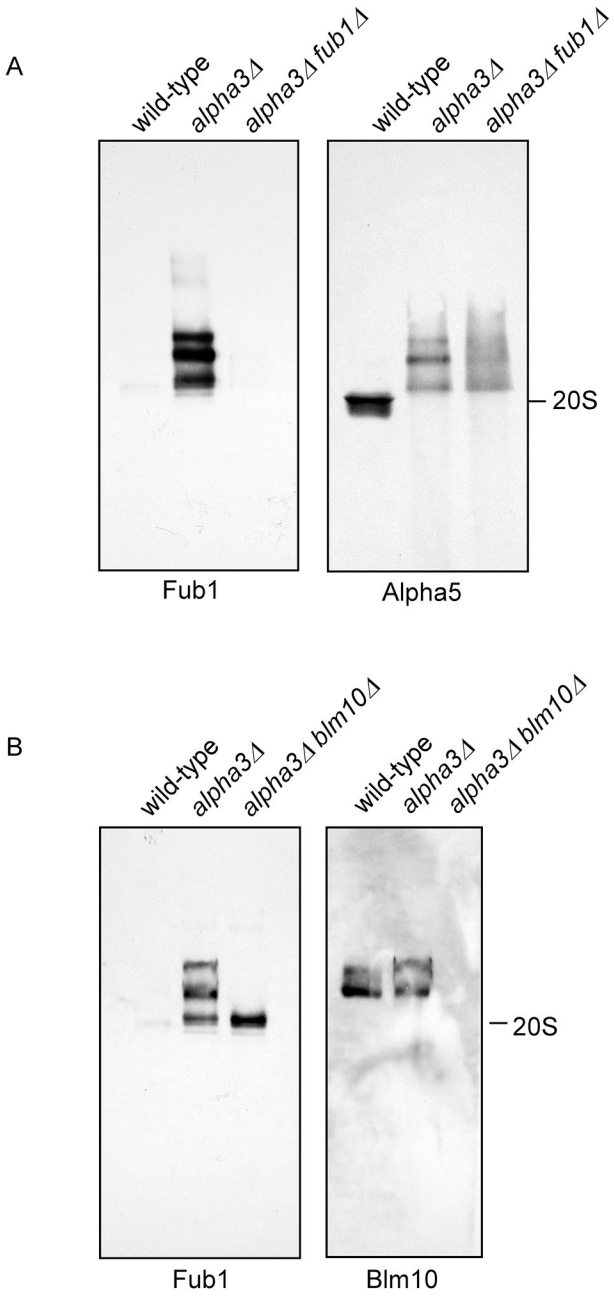

Extended Data Fig. 2. Additional Analysis of Fub1 Binding to *alpha3*Δ CP.

a, Purified CP (1.4 μg) from the indicated strains was analyzed by native gel electrophoresis followed by immunoblotting with antibodies recognizing Fub1 and Alpha5. These results confirm that the Fub1-immunoreactive species do indeed represent Fub1. **b**, Purified CP (1.1 μg) from the indicated strains was analyzed by native gel electrophoresis followed by immunoblotting with antibodies recognizing Fub1 and Blm10. These results indicate that the two supra-20S species contain Blm10. The identity of the highest molecular weight species, however, remains uncertain as doubly Blm10-capped CP was not visualized by cryo-EM (see Extended Data Fig. 3, below). Similar results were obtained in two independent experiments.

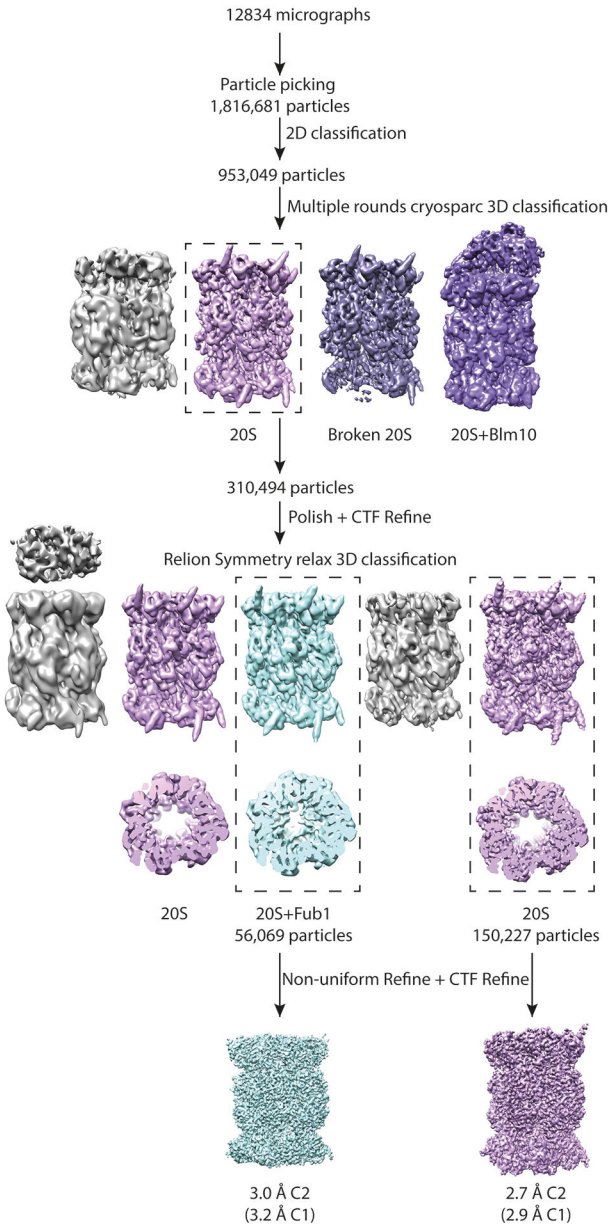

Extended Data Fig. 3. Cryo-EM Classification of CP Species.

Processing scheme for classification and refinement of proteasome species. “Junk” classes are colored grey while identifiable species are colored by species. All 3D classification steps were carried out in cryoSPARC.

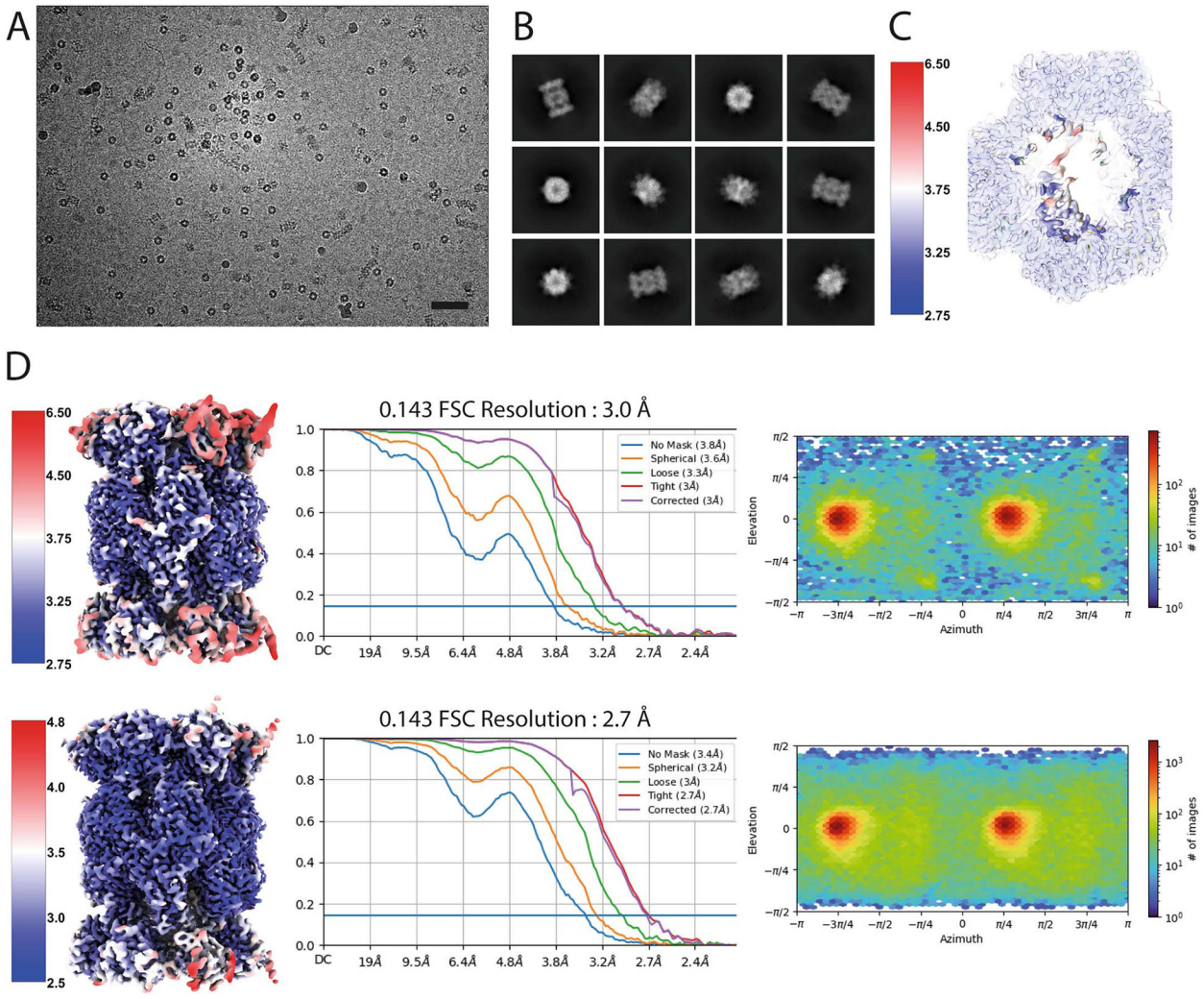

Extended Data Fig. 4. Cryo-EM Data Analysis for CP Species.

a, Representative micrograph of proteasome particles embedded in vitreous ice. Scale bar = 500 Å. A total of 12,834 micrographs were collected from a single multi-day experiment. **b**, Selected 2D class averages of 20S particles. **c,** Local resolution slice through the *α3Δ* + Fub1 containing reconstruction. Local resolution values vary between ~3.0 - 5.0 Å in this region. CP density around Fub1 is shown for orientation. **d**, Reconstructions of Fub1-containing (top panels) and Fub1-lacking (bottom panels) CP filtered and colored by local resolution (left), gold-standard Fourier shell correlation (FSC) curves from cryoSPARC (middle), and viewing direction distribution plots (right). Resolution determined at FSC = 0.143.

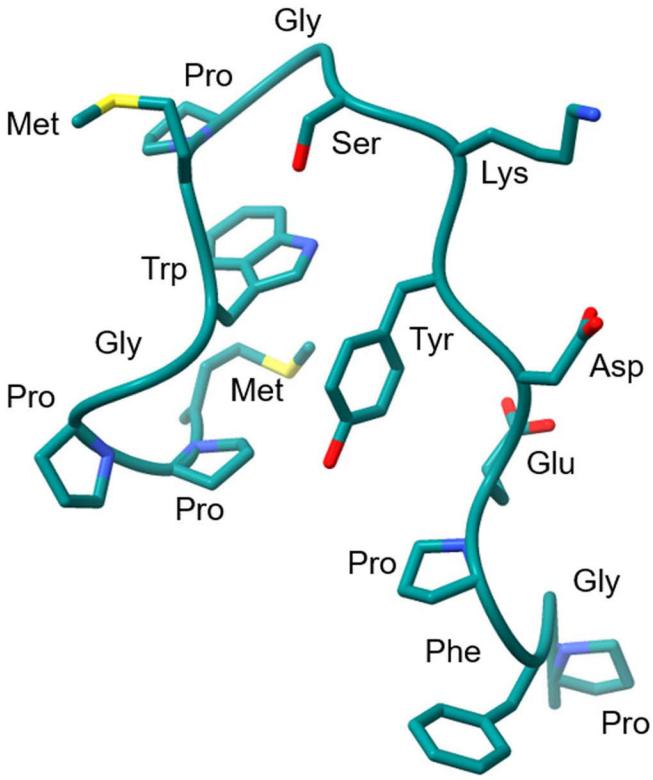

		β2 Inhibition
1. Fub1 (213-232)	MPPGWMPGSKYDEPFGPGSG	++++
2. Fub1 (213-227)	MPPGWMPGSKYDEPF	++++
3. Fub1 (213-223)	MPPGWMPGSKY	-
4. Fub1 (217-230)	WMPGSKYDEPFGPG	++
5. Fub1 (221-227)	SKYDEPF	-

Extended Data Fig. 5. Further Analysis of β2 Inhibition by Fub1 Peptides.
Mapping of the inhibitory effect of the β2 peptide. The structure of this part of Fub1 is shown above, although the last three residues were not resolved.

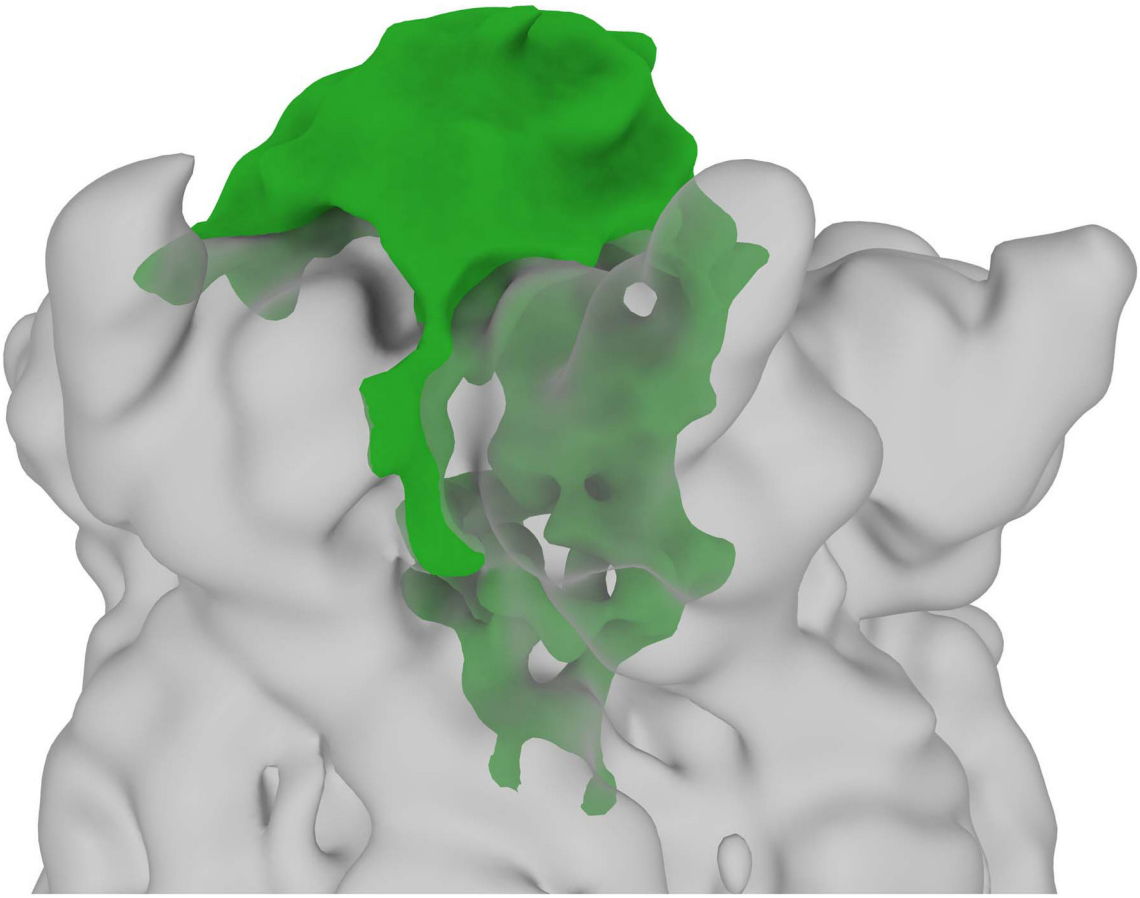

Extended Data Fig. 6. Additional Low Resolution Density in the *α3Δ* + Fub1 Structure.
Shown is the same low pass filtered map from Fig. 7d. In addition to the capping density shown in Fig. 7d, there is further density from difference maps (shown in green) within the CP barrel that extends through the α-ring and into the β-ring. Difference density has been further gaussian filtered and additional unconnected density omitted for clarity.

Supplementary Material

Refer to Web version on PubMed Central for supplementary material.

Acknowledgements

We thank David Waterman and Daniel Finley for early contributions to the project, and Daniel Finley for assistance with chromatography, helpful advice, and comments on the manuscript. We thank Jeroen Roelofs for the Pba1/2 antibody. This work was supported by NIH grants R01-GM144367 (to J.H.), DP5-OD019800 (to J.H.), R01-GM074830 (to L.H.), and R01-GM130144 (to L.H.).

Data availability

Cryo-EM maps and atomic model coordinates have been deposited in the Electron Microscopy Data Bank and the Protein Data Bank, respectively: *α3Δ* 20S (EMD-25847, PDB 7TEJ) and *α3Δ* 20S+Fub1 Complex (EMDB-25848, PDB 7TEO). Additional

structures referenced here include 3MG0, 5CZ4, and 7LS5. Source data are provided with this paper.

References

1. Bard JAM et al. Structure and Function of the 26S Proteasome. Annu. Rev. Biochem 87, 697–724 (2018). [PubMed: 29652515]
2. Rousseau A & Bertolotti A Regulation of proteasome assembly and activity in health and disease. Nat. Rev. Mol. Cell Biol 19, 697–712 (2018). [PubMed: 30065390]
3. Tomko RJ & Hochstrasser M Molecular architecture and assembly of the eukaryotic proteasome. Ann. Rev. Biochem 82, 415–445 (2013). [PubMed: 23495936]
4. Hanna J et al. Deubiquitinating Enzyme Ubp6 Functions Noncatalytically to Delay Proteasomal Degradation. Cell 127, 99–111 (2006). [PubMed: 17018280]
5. Crosas B et al. Ubiquitin Chains Are Remodeled at the Proteasome by Opposing Ubiquitin Ligase and Deubiquitinating Activities. Cell 127, 1401–1413 (2006). [PubMed: 17190603]
6. Hanna J, Waterman D, Boselli M & Finley D Spg5 protein regulates the proteasome in quiescence. J. Biol. Chem 287, 34400–34409 (2012). [PubMed: 22904326]
7. Hanna J et al. Cuz1/Ynl155w, a Zinc-dependent ubiquitin-binding protein, protects cells from metalloid-induced proteotoxicity. J. Biol. Chem 289, 1876–1885 (2014). [PubMed: 24297164]
8. Sá-Moura B et al. A conserved protein with AN1 zinc finger and ubiquitin-like domains modulates Cdc48 (p97) function in the ubiquitin-proteasome pathway. J. Biol. Chem 288, 33682–33696 (2013). [PubMed: 24121501]
9. Lee D, Takayama S & Goldberg AL ZFAND5/ZNF216 is an activator of the 26S proteasome that stimulates overall protein degradation. PNAS USA 115, E9550–E9559 (2018). [PubMed: 30254168]
10. Shi Y et al. Rpn1 provides adjacent receptor sites for substrate binding and deubiquitination by the proteasome. Science (1979) 351, (2016).
11. Chu-Ping M, Slaughter CA & Demartino GN Purification and characterization of a protein inhibitor of the 20S proteasome (macropain). Biochim. Biophys. Acta 1119, 303–311 (1992). [PubMed: 1312359]
12. Hatanaka A et al. Fub1p, a novel protein isolated by boundary screening, binds the proteasome complex. Genes Genet. Syst 86, 305–314 (2011). [PubMed: 22362029]
13. Zaiss DMW et al. The proteasome inhibitor PI31 competes with PA28 for binding to 20S proteasomes. FEBS Lett. 457, 333–338 (1999). [PubMed: 10471803]
14. McCutchen-Maloney SL et al. cDNA cloning, expression, and functional characterization of PI31, a proline-rich inhibitor of the proteasome. J. Biol. Chem 275, 18557–18565 (2000). [PubMed: 10764772]
15. Yashiroda H et al. N-Terminal α7 Deletion of the Proteasome 20S Core Particle Substitutes for Yeast PI31 Function. Mol. Cell. Biol 35, 141–152 (2015). [PubMed: 25332237]
16. Velichutina I, Connerly PL, Arendt CS, Li X & Hochstrasser M Plasticity in eucaryotic 20S proteasome ring assembly revealed by a subunit deletion in yeast. EMBO J 23, 500–510 (2004). [PubMed: 14739934]
17. Emori Y et al. Molecular Cloning and Functional Analysis of Three Subunits of Yeast Proteasome. Mol. Cell. Biol 11, 344–353 (1991). [PubMed: 1898763]
18. Sadre-Bazzaz K, Whitby FG, Robinson H, Formosa T & Hill CP Structure of a Blm10 Complex Reveals Common Mechanisms for Proteasome Binding and Gate Opening. Mol. Cell 37, 728–735 (2010). [PubMed: 20227375]
19. Toste Rêgo A & da Fonseca PCA Characterization of Fully Recombinant Human 20S and 20S-PA200 Proteasome Complexes. Mol. Cell 76, 138–147.e5 (2019). [PubMed: 31473102]
20. Guerra-Moreno A & Hanna J Tmc1 is a dynamically regulated effector of the Rpn4 proteotoxic stress response. J. Biol. Chem 291, 14788–14795 (2016). [PubMed: 27226598]

21. Edskes HK, Stroobant EE, DeWilde MP, Bezsonov EE & Wickner RB Proteasome control of [URE3] prion propagation by degradation of anti-prion proteins Cur1 and Btn2 in saccharomyces cerevisiae. Genetics 218, (2021).
22. Blackburn C et al. Characterization of a new series of non-covalent proteasome inhibitors with exquisite potency and selectivity for the 20S β5-subunit. Biochem. J 430, 461–476 (2010). [PubMed: 20632995]
23. Huber EM et al. Systematic Analyses of Substrate Preferences of 20S Proteasomes Using Peptidic Epoxyketone Inhibitors. J Am Chem Soc 137, 7835–7842 (2015). [PubMed: 26020686]
24. Köhler A et al. The Axial Channel of the Proteasome Core Particle Is Gated by the Rpt2 ATPase and Controls Both Substrate Entry and Product Release. Mol. Cell 7, 1143–1152 (2001). [PubMed: 11430818]
25. Kirk R et al. Structure of a conserved dimerization domain within the F-box protein Fbxo7 and the PI31 proteasome inhibitor. J. Biol. Chem 283, 22325–22335 (2008). [PubMed: 18495667]
26. Kao A et al. Development of a Novel Cross-linking Strategy for Fast and Accurate Identification of Cross-linked Peptides of Protein Complexes. Molecular & Cellular Proteomics 10, M110.002170 (2011).
27. Bode W, and Huber R. Natural protein proteinase inhibitors and their interaction with proteinases. Eur. J. Biochem 204, 433–51 (1992). [PubMed: 1541261]
28. Schnell HM et al. Structures of chaperone-associated assembly intermediates reveal coordinated mechanisms of proteasome biogenesis. Nat. Struct. Mol. Biol 28, 418–425 (2021). [PubMed: 33846632]
29. Shang J, Huang X & Du Z The FP domains of PI31 and Fbxo7 have the same protein fold but very different modes of protein-protein interaction. J. Biomol. Struct. Dyn 33, 1528–1538 (2014). [PubMed: 25266262]
30. Li X, Thompson D, Kumar B & DeMartino GN Molecular and cellular roles of PI31 (PSMF1) protein in regulation of proteasome function. Journal of Biological Chemistry 289, 17392–17405 (2014). [PubMed: 24770418]
31. Liu CW, Corboy MJ, DeMartino GN & Thomas PJ Endoproteolytic activity of the proteasome. Science (1979) 299, 408–411 (2003).
32. Groll M et al. Structure of 20S proteasome from yeast at 2.4A resolution. Nature 386, 463–471 (1997). [PubMed: 9087403]
33. Kulak NA, Pichler G, Paron I, Nagaraj N & Mann M Minimal, encapsulated proteomic-sample processing applied to copy-number estimation in eukaryotic cells. Nature Methods 11, 319–324 (2014). [PubMed: 24487582]
34. Cho-Park PF & Steller H Proteasome regulation by ADP-ribosylation. Cell 153, 614–627 (2013). [PubMed: 23622245]
35. Liu K et al. PI31 Is an Adaptor Protein for Proteasome Transport in Axons and Required for Synaptic Development. Dev. Cell 50, 509–524.e10 (2019). [PubMed: 31327739]
36. Zhao L et al. A Rare Variant Nonparametric Linkage Method for Nuclear and Extended Pedigrees with Application to Late-Onset Alzheimer Disease via WGS Data. American Journal of Human Genetics 105, 822–835 (2019). [PubMed: 31585107]
37. Minis A et al. The proteasome regulator PI31 is required for protein homeostasis, synapse maintenance, and neuronal survival in mice. PNAS 116, 24639–24650 (2019). [PubMed: 31754024]

Methods-Only References

38. Wani PS, Rowland MA, Ondracek A, Deeds EJ & Roelofs J Maturation of the proteasome core particle induces an affinity switch that controls regulatory particle association. Nat. Comm 6, (2015).
39. Leggett DS et al. Multiple Associated Proteins Regulate Proteasome Structure and Function. Mol. Cell 10, 495–507 (2002). [PubMed: 12408819]
40. Mastronarde DN Automated electron microscope tomography using robust prediction of specimen movements. J. Struct. Biol 152, 36–51 (2005). [PubMed: 16182563]

41. Zheng SQ et al. MotionCor2: Anisotropic correction of beam-induced motion for improved cryo-electron microscopy. Nat. Methods 14, 331–332 (2017). [PubMed: 28250466]
42. Rohou A & Grigorieff N CTFFIND4: Fast and accurate defocus estimation from electron micrographs. J. Struct. Biol 192, 216–221 (2015). [PubMed: 26278980]
43. Wagner T et al. SPHIRE-crYOLO is a fast and accurate fully automated particle picker for cryo-EM. Commun. Biol 2:218, (2019). [PubMed: 31240256]
44. Scheres SHW RELION: Implementation of a Bayesian approach to cryo-EM structure determination. J. Struct. Biol 180, 519–530 (2012). [PubMed: 23000701]
45. Punjani A, Rubinstein JL, Fleet DJ & Brubaker MA CryoSPARC: Algorithms for rapid unsupervised cryo-EM structure determination. Nat. Methods 14, 290–296 (2017). [PubMed: 28165473]
46. Morin A et al. Collaboration gets the most out of software. Elife 2:e01456, (2013). [PubMed: 24040512]
47. Pettersen EF et al. UCSF Chimera - A visualization system for exploratory research and analysis. J. Comput. Chem 25, 1605–1612 (2004). [PubMed: 15264254]
48. Emsley P, Lohkamp B, Scott WG & Cowtan K Features and development of Coot. Acta Cryst. D66, 486–501 (2010).
49. Croll TI ISOLDE: A physically realistic environment for model building into low-resolution electron-density maps. Acta Cryst. D74, 519–530 (2018).
50. Liebschner D et al. Macromolecular structure determination using X-rays, neutrons and electrons: Recent developments in Phenix. Acta Cryst. D75, 861–877 (2019).
51. Pfab J, Phan M & Si D DeepTracer for fast de novo cryo-EM protein structure modeling and special studies on CoV-related complexes. BIOPHYSICS AND COMPUTATIONAL BIOLOGY 118, 2021 (2021).
52. Celniker G et al. ConSurf: Using evolutionary data to raise testable hypotheses about protein function. Isr. J. Chem 53, 199–206 (2013).
53. Ashkenazy H et al. ConSurf 2016: an improved methodology to estimate and visualize evolutionary conservation in macromolecules. Nucleic acids res. 44, W344–W350 (2016). [PubMed: 27166375]
54. Gutierrez CB et al. Developing an acidic residue reactive and sulfoxide-containing MS-cleavable homobifunctional cross-linker for probing protein-protein interactions. Analytical Chemistry 88, 8315–8322 (2016). [PubMed: 27417384]
55. Daniel Gietz R & Sugino A New yeast-Escherichia coli shuttle vectors constructed with in vitro mutagenized yeast genes lacking six-base pair restriction sites. Gene 74, 527–534 (1988). [PubMed: 3073106]

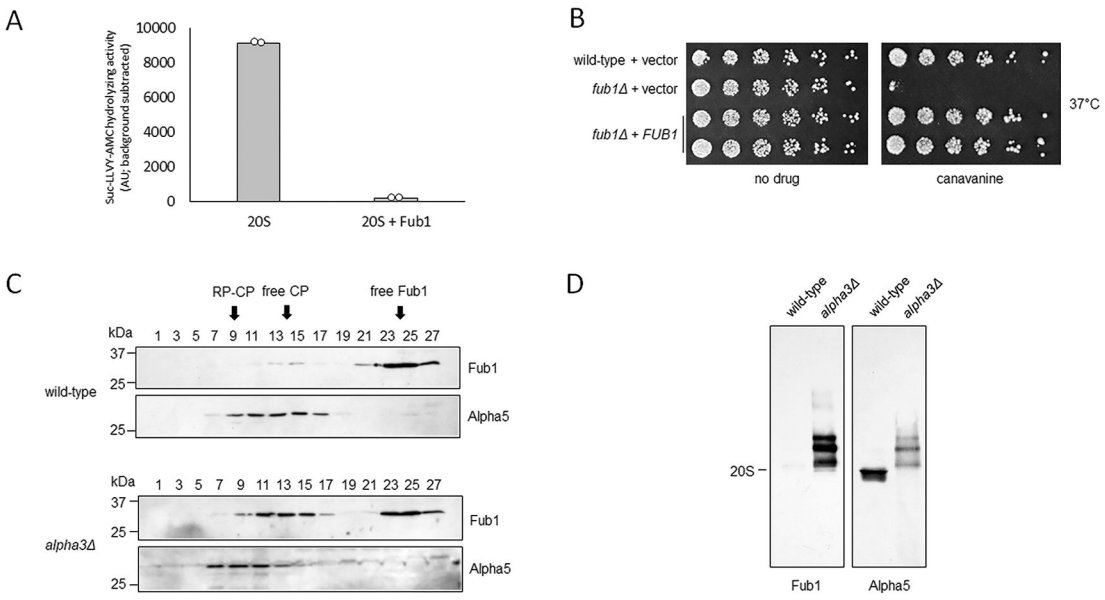

Fig. 1 |. Enrichment of Fub1 in the *alpha3*Δ Mutant.

a, CP (15 nM) enzymatic activity in the presence or absence of Fub1 (25-fold molar excess) as determined using the fluorogenic substrate suc-LLVY-AMC. Open circles indicate individual data points from biologic replicates. **b**, Growth of the indicated strains on selective media in the presence or absence of canavanine (1.5 μg/mL). Cells were spotted in 3-fold serial dilutions and cultured at 37°C for 2-7 days. Similar results were obtained in ten independent experiments. **c**, Size exclusion chromatography of clarified whole cell extracts from the indicated strains. The indicated fractions were analyzed by SDS-PAGE and immunoblotting with antibodies recognizing Fub1 and the CP subunit Alpha5. Heavier material runs to the left. Similar results were obtained in two independent experiments. **d**, Purified CP (0.9 μg) from the indicated strains was analyzed by native gel electrophoresis followed by immunoblotting with antibodies recognizing Fub1 and Alpha5. Similar results were obtained in five independent experiments. Uncropped images for panel c and data for graph in panel a are available as source data.

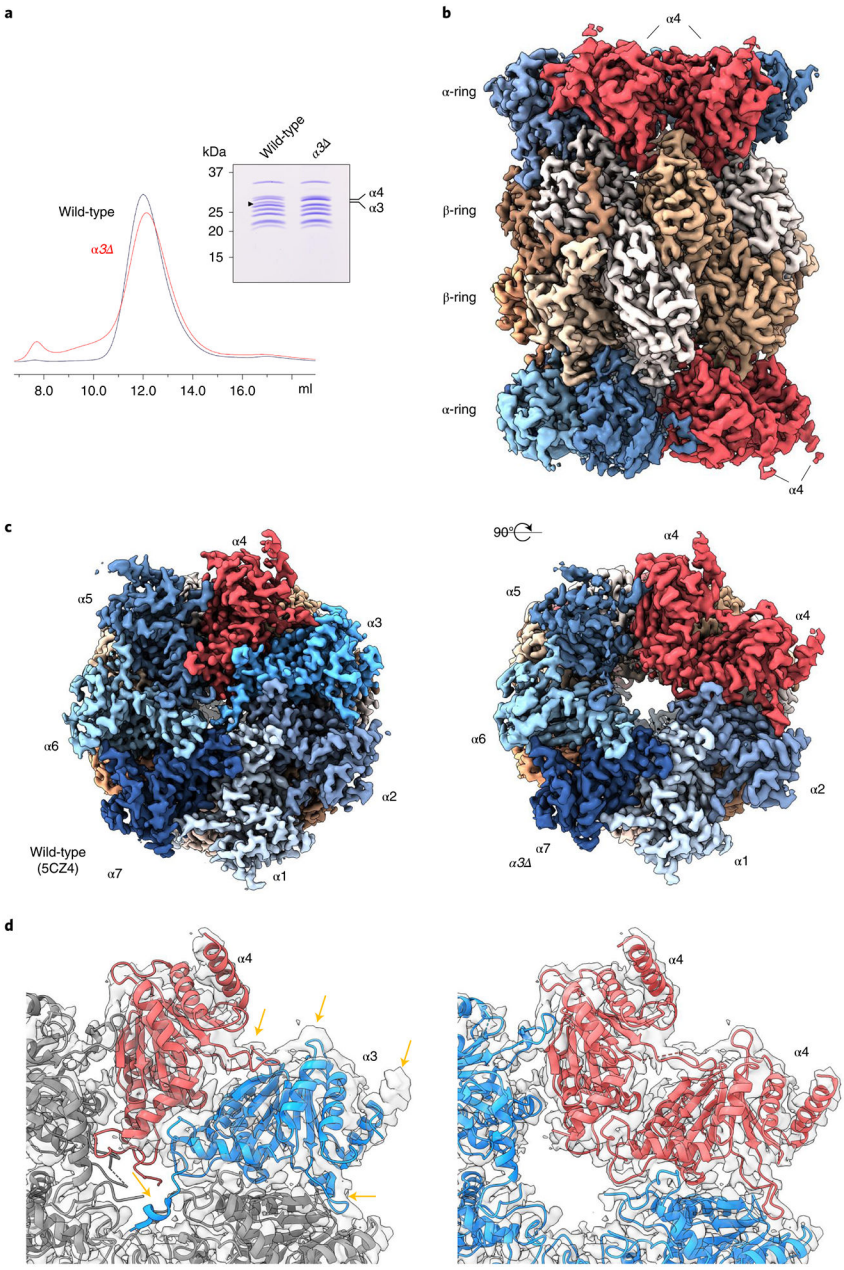

Fig. 2 | *α3Δ* CP Shows an Open Gate Due to Aberrant α-ring Composition.

a, Electrophoretic profile and size exclusion chromatography of purified CP from wild-type and *α3Δ*. Arrowhead denotes α3. Similar results were obtained in five independent experiments. **b**, Side view of *α3Δ* CP (2.7 Å). **c**, Top view comparing wild-type CP (5CZ4) and *α3Δ* CP. Note the constitutively open gate in *α3Δ* CP. **d**, Modeling of the *α3Δ* CP confirms that a second copy of α4 is present at the position normally occupied by α3. Yellow arrows indicate areas of the density incompatible with α3. Uncropped image for panel a is available as source data.

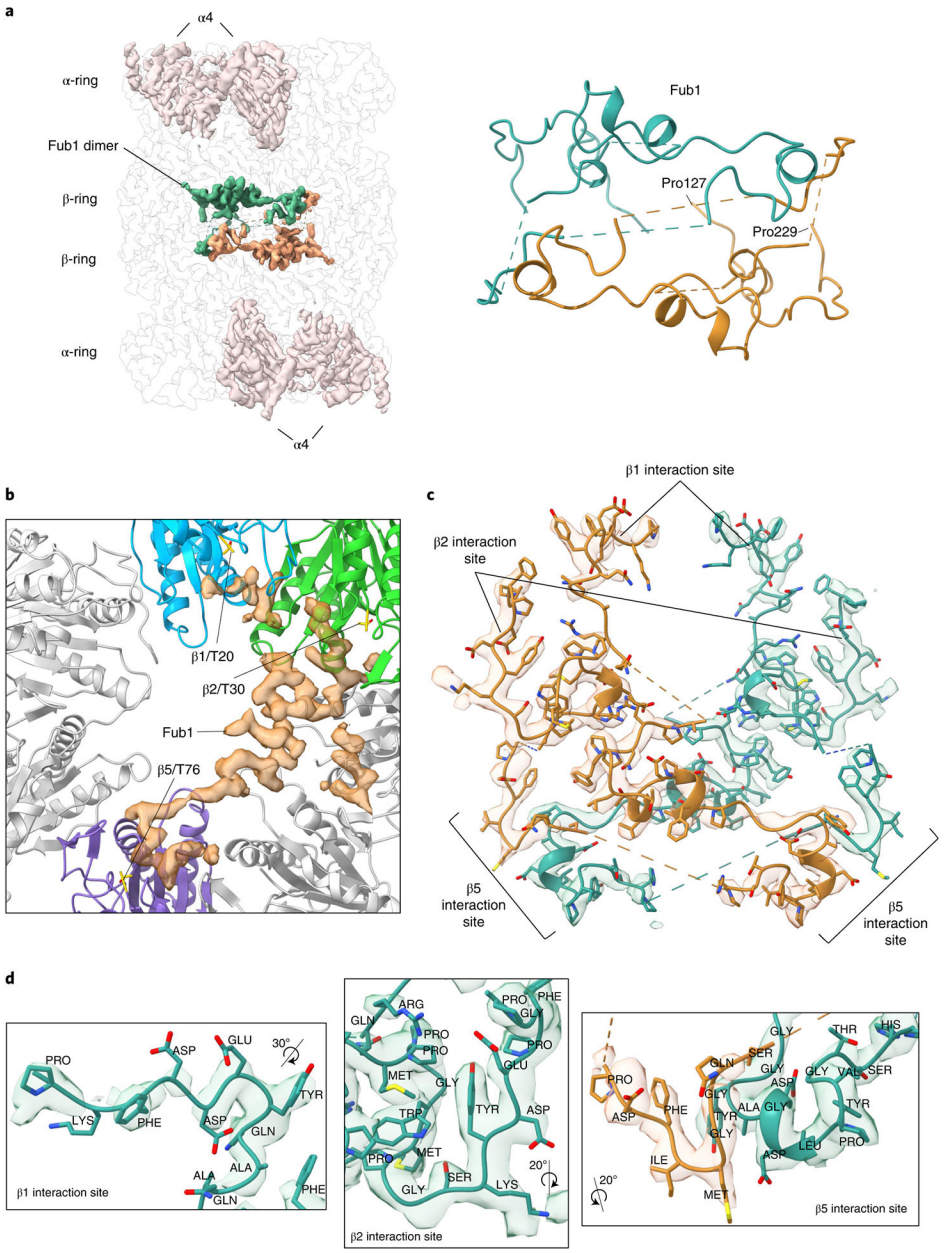

Fig. 3 |. Cryo-EM Structure of Fub1-bound CP.

a, Structure of *α3Δ* CP (3.0 Å) with a novel central density that corresponds to Fub1. The extra copies of α4 are indicated. Shown to the right is the modeled structure of the Fub1 dimer with the first and last resolved residues listed. **b**, Fub1 interacts with and occupies all of the active site pockets. For clarity, the Fub1 density is shown with only one of the β-rings and the second Fub1 protein has been omitted. Active site threonines are labeled. **c**, The Fub1 model is shown overlaid onto the primary cryo-EM map density. Dimerization occurs near each β5 active site. Regions interacting with the indicated β-subunit active sites are indicated. **d**, Close-up views of Fub1 confirming that the density closely matches the modeled amino acid side chains of Fub1.

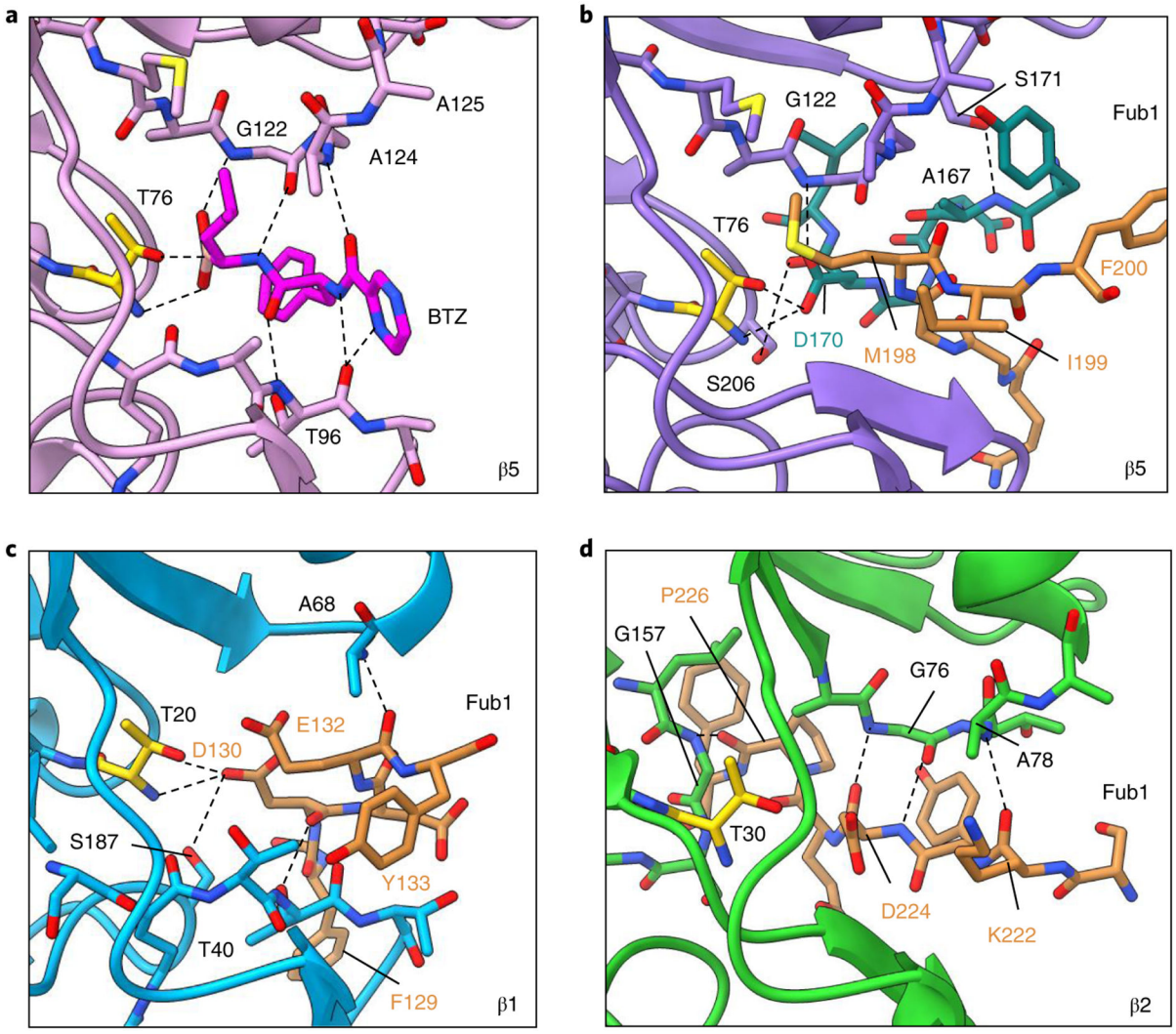

Fig. 4 | Interaction of Fub1 with Proteasome Active Sites.

a, Interaction of the modified dipeptide proteasome inhibitor bortezomib with the β5 active site pocket (3MG0). **b**, Fub1's interaction with the β5 active site pocket mirrors many of the interactions seen in panel A. **c**, Close-up view of Fub1 with the β1 active site. **d**, Close-up view of Fub1 with the β2 active site. Dashed lines indicate hydrogen bonds.

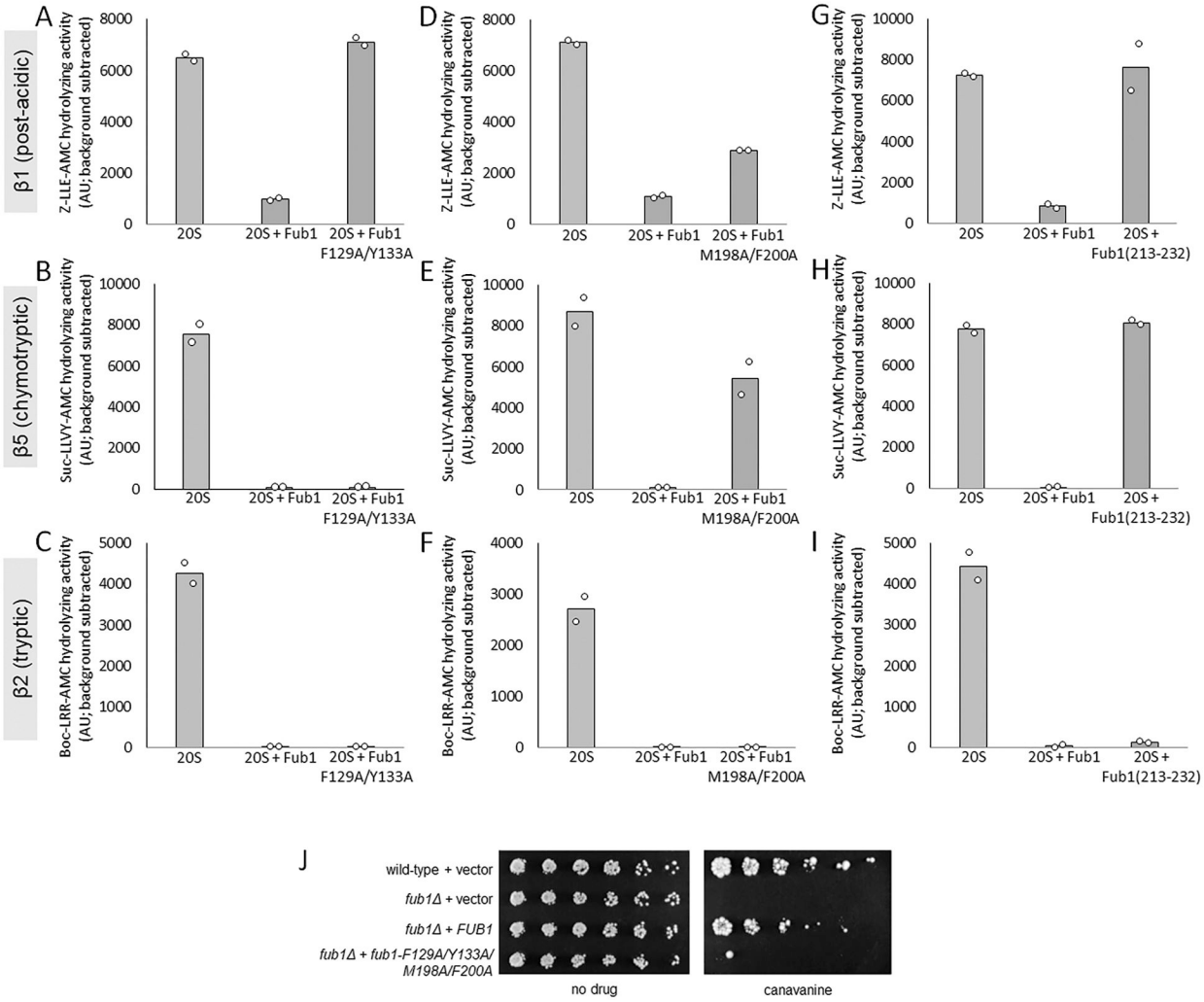

Fig. 5 | Inhibition of Individual CP Active Sites by Fub1.

a-c, CP (15 nM) enzymatic activity in the presence or absence of Fub1 (25-fold molar excess) as determined using the fluorogenic substrates Z-LLE-AMC (β1), suc-LLVY-AMC (β5), and Boc-LRR-AMC (β2). **d-f**, CP (15 nM) activity in the presence or absence of Fub1 (25-fold molar excess) as determined using the three fluorogenic substrates. **g-i**, CP (15 nM) activity in the presence or absence of Fub1(213-232) peptide (50 μm) as determined using the three fluorogenic substrates. AU, arbitrary units. Open circles indicate individual data points from biologic replicates. **j**, Growth of the indicated strains on selective media in the presence or absence of canavanine (1.5 μg/mL). Cells were spotted in 3-fold serial dilutions and cultured at 37°C for 3-7 days. Similar results were obtained in three independent experiments. Data for graphs in panels a-i are available as source data.

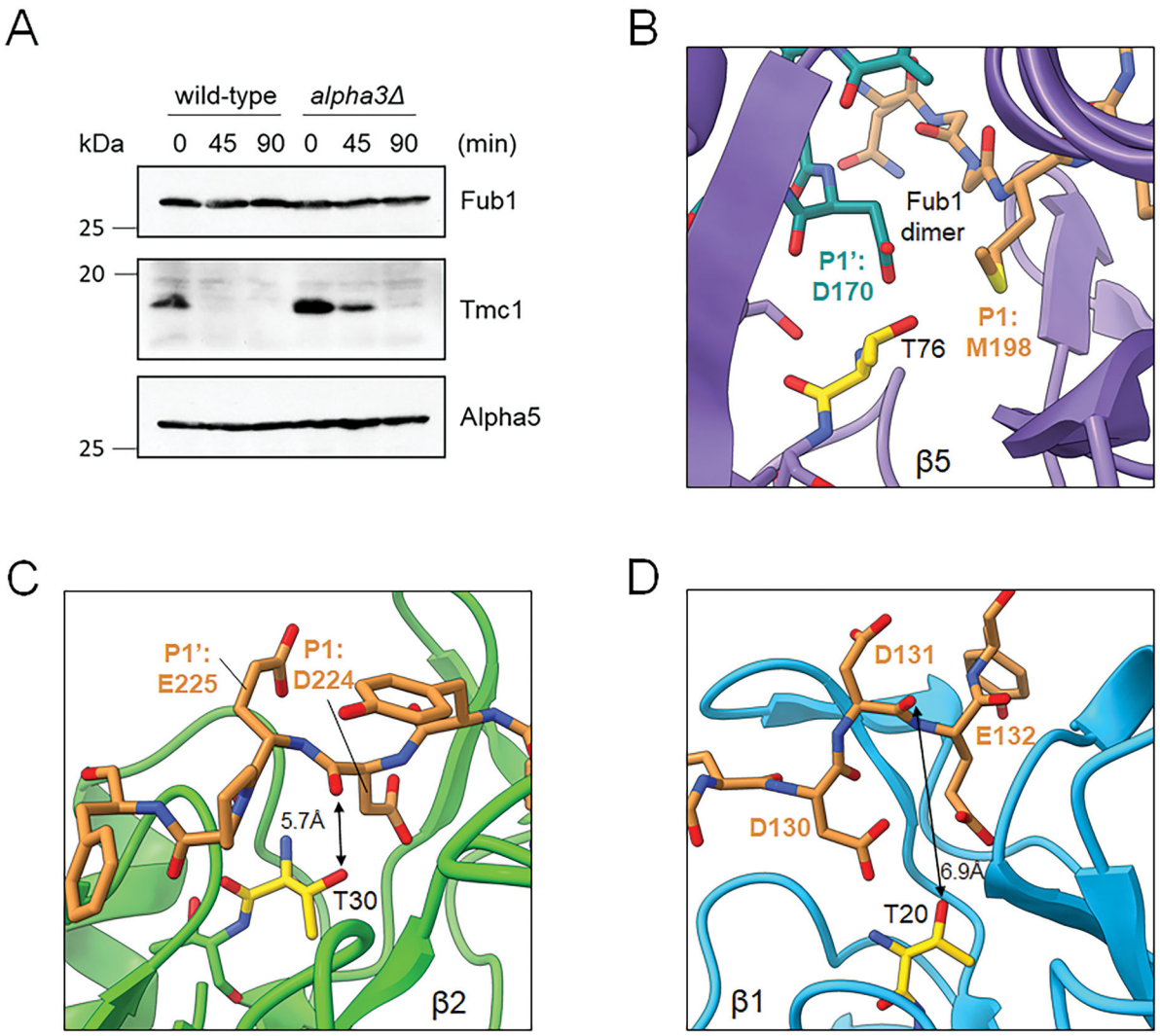

Fig. 6 | Fub1 Evades Degradation by Distinct Mechanisms at Each Active Site.

a, Cycloheximide chase analysis of Fub1 stability. Cycloheximide (100 μg/ml) was added at time zero, and whole-cell extracts were prepared and analyzed by SDS-PAGE followed by immunoblotting with the indicated antibodies. Similar results were obtained in three independent experiments. **b**, Positioning of Fub1 in the active site pocket of β5. Fub1 residues corresponding to the P1 and P1' positions were determined by comparison to structures of CP bound to peptide inhibitors. The active site Thr76 is indicated. **c**, Positioning of Fub1 in the active site pocket of β2. The active site Thr30 is indicated. **d**, Positioning of Fub1 in the active site pocket of β1; Fub1 is oriented in the opposite direction relative to other CP-inhibitor structures. The active site Thr20 is indicated. The distance between the active site Thr and the polypeptide main chain is indicated by the double-sided arrow (panels c,d). Uncropped images for panel a are available as source data.

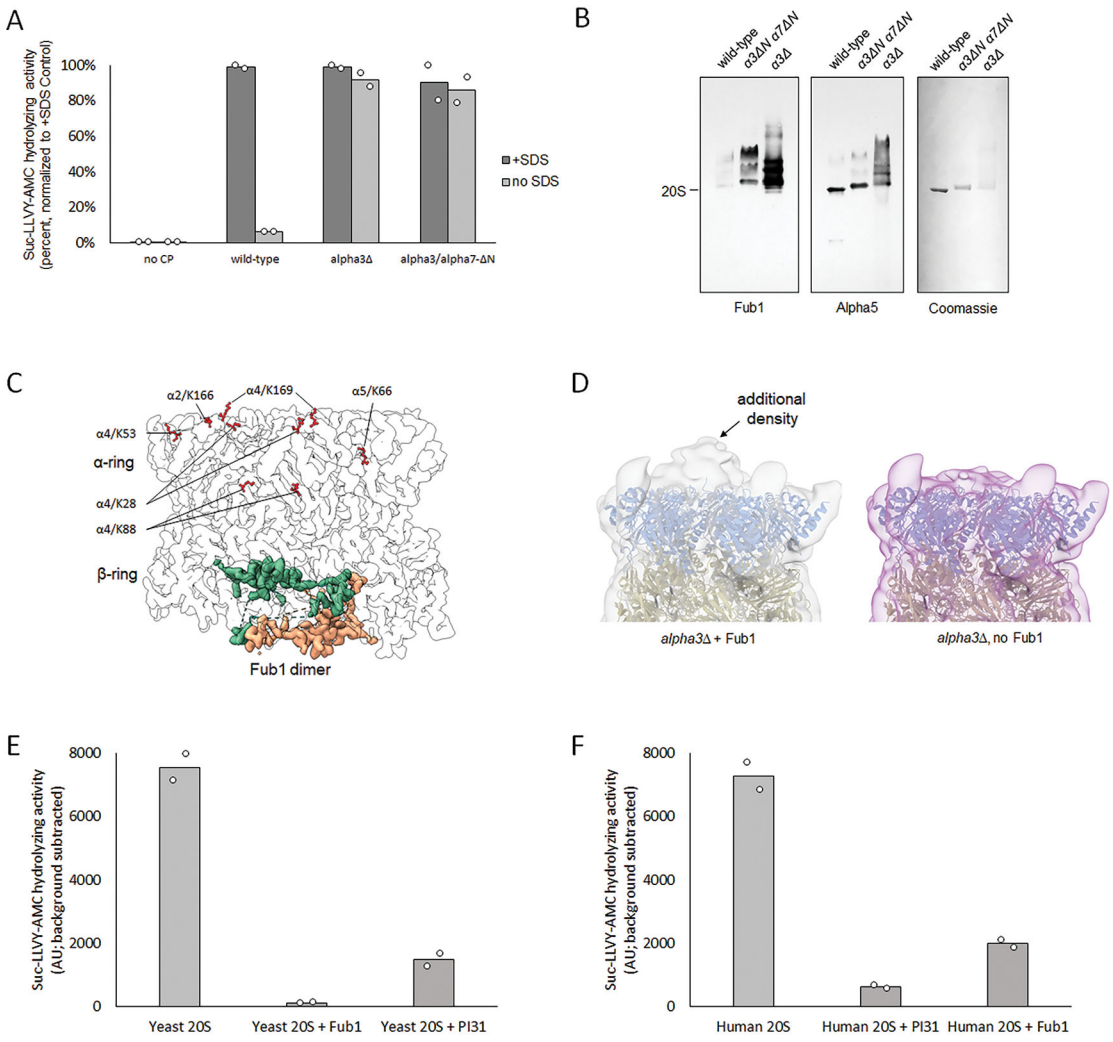

Fig. 7 | Fub1 is Enriched in Open Gate CP Mutants and its Ability to Inhibit CP is Evolutionarily Conserved.

a, CP (15 nM) enzymatic activity of the indicated strains in the presence or absence of SDS (0.02%) as determined using the fluorogenic substrate suc-LLVY-AMC. **b**, Purified CP (1.7 μg) from the indicated strains was analyzed by native gel electrophoresis followed by immunoblotting with antibodies against Fub1 and Alpha5. Right panel, Coomassie-stained gel. Similar results were obtained in two independent experiments. **c**, Crosslinks between Fub1 and CP subunits as determined by cross-linking mass spectrometry. **d**, Electron density maps (low pass filtered to 10Å) of *a3Δ* CP with and without Fub1. The additional density is indicated. **e**, Yeast CP (15 nM) enzymatic activity in the presence or absence of yeast Fub1 or human PI31 (25-fold molar excess) as determined using the fluorogenic substrate suc-LLVY-AMC. **f**, Human CP (10 nM) enzymatic activity in the presence or absence of human PI31 or yeast Fub1 (37.5-fold molar excess). In panels a, e and f, open circles indicate individual data points from biologic replicates. Data for graphs in these panels are available as source data.

Table 1:

Cryo-EM data collection, refinement and validation statistics

	Alpha3Δ (EMD-25847, PDB 7TEJ)		Alpha3Δ+Fub1 (EMD-25848, PDB 7TEO)
Data collection and processing			
Magnification		47,169	
Voltage (kV)		300	
Electron exposure (e^{-}/Å^{-2})		53.85	
Defocus range (μm)		0.8, 2.2	
Pixel size (Å)		1.06	
Symmetry imposed	C2		C2
Initial particle images (no.)		953,049	
Final particle images (no.)	150,227		56,059
Map Resolution (Å)	2.7		3.0
FSC threshold		0.143	
Map resolution range (Å)	2.5-5.2		2.7-6.3
Refinement			
Initial model used	7LS5		Alpha3Δ
Model resolution (Å)	2.90		3.20
FSC threshold	0.500		0.500
Map-sharpening B-factor (Å^2)	−80.9		−72.2
Model composition			
Non-hydrogen atoms	45,748		48,916
Protein residues	5,863		6,288
B factors (Å2)			
Protein	46.32		56.46
R.M.S.D. deviations			
Bond lengths (Å)	0.004		0.003
Bond angles (°)	0.582		0.548
Validation			
MolProbity score	1.24		1.22
Clashscore	4.73		4.46
Poor rotamers (%)	0		0.00
Ramachandran plot			
Favored (%)	98.60		98.45
Allowed (%)	1.40		1.22
Disallowed (%)	0		0